Electronic Supplementary Material (ESI) for Nanoscale.

Supporting Information

Interfacial synergy between dispersed Ru sub-nanoclusters and porous NiFe layered double hydroxide on accelerated overall water splitting by intermediate modulation

Yao Wang,[a] Peng Zheng,[a] Mingxuan Li,[a] Yunrui Li,[a] Xin Zhang,[a,*] Juan Chen,[a] Xu Fang,[a] Yujie Liu,[a] Xiaolin Yuan,[a] Xiaoping Dai,[a] Hai Wang[b]

[a]State Key Laboratory of Heavy Oil Processing, College of Chemical Engineering and Environment, China University of Petroleum, Beijing 102249, China

Corresponding author: Xin Zhang* E-mail: zhangxin@cup.edu.cn;

[b]National Institute of Metrology, Beijing 100013, China

The method of ECSA measurement

The electrochemical surface area was measured from its electrochemical capacitance in a non-faradic region. By plotting the capacitive currents (J_{anodic} - $J_{cathodic}$)/2 vs. v, the capacitance can be estimated as half of the slope. The C_{dl} is believed to provide meaningful results for the comparison of real active surface area owing to the accessible surface sites can be fully exposed to electrolyte.

Computational methods and models

All calculations were performed using DMol^3 program package. The exchange-correlation energy was calculated within the generalized gradient approximation (GGA). In addition, the Perdew-Burke-Ernzerhof (PBE) function with the Grimme method for DFT-D correction was used to evaluate the intermolecular force. The maximum force applied in the geometry optimization was 2.0×10^{-3} Ha/Å. The k-points of (3×3×1), the orbital cutoff of 5.5 Å and the vacuum region of 15 Å were used in all calculations. Spin states were explicitly set. In this calculation, the Ru@$Ni(OH)_2$ and RuO_2@NiOOHx were generated on the basis of the $Ni(OH)_2$ and NiO_2 slab models, where the $Ni(OH)_2$ and NiO_2 were composed of 4 Ni rows in the x-direction and 4 Ni rows in the y-direction. The Ru cluster model for Ru@$Ni(OH)_2$ is composed of 13 atoms with a diameter of 7.40 Å. The Ru (100) surface was modeled by periodically repeated four-layer slabs. The atoms in the top two layers were relaxed, while the rest of the atoms were fixed in the positions. The adsorption energies (E_{ads}) were calculated using the equation as follows, where $E_{adsorbent/slab}$ was the total energy of the adsorbate interacting with the slab, $E_{adsorbent}$ and E_{slab} were the energies of the free adsorbate in gas phase and the bare slab, respectively.

$$E_{ads} = E_{adsorbent/slab} - E_{adsorbent} - E_{slab}$$

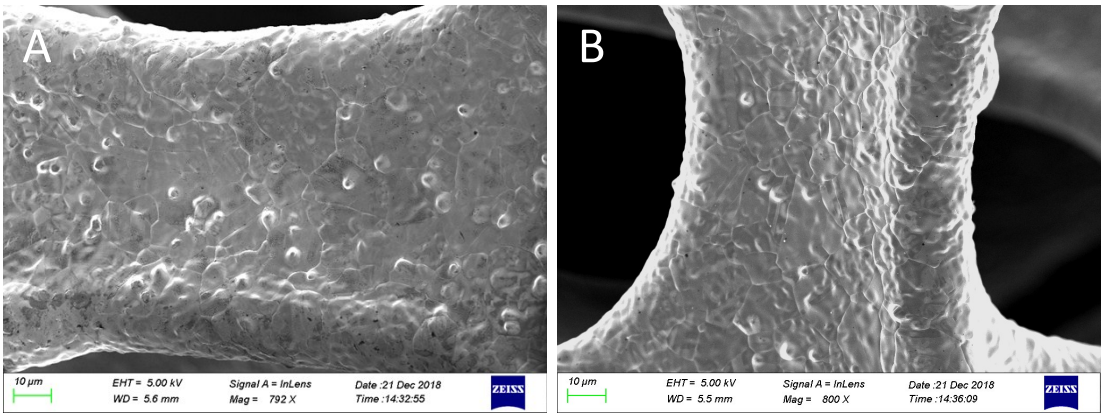

Figure S1. SEM images of NF: (A) pristine NF, and (B) cleaned NF.

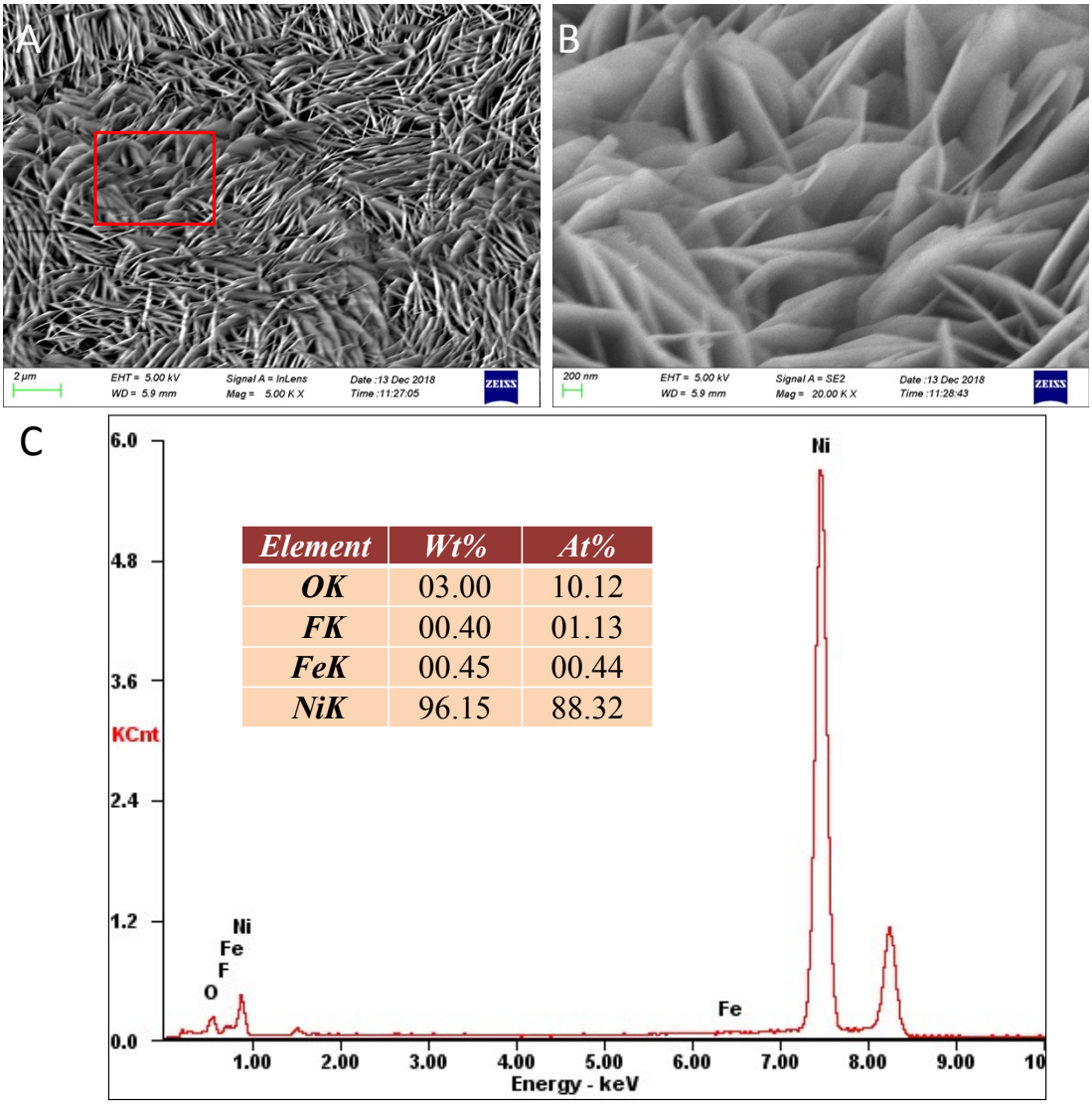

Figure S2. (A, B)SEM images and (C) EDX analysis of NiFe LDH-F/NF catalyst.

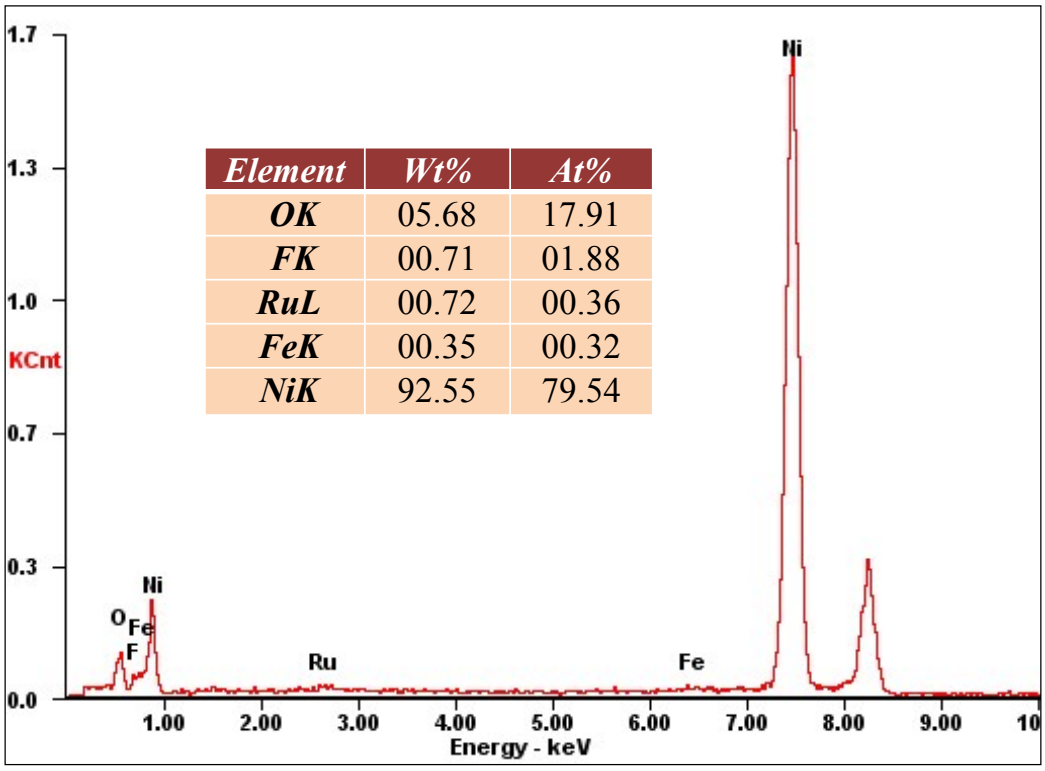

Element	*Wt%*	*At%*
OK	05.68	17.91
FK	00.71	01.88
RuL	00.72	00.36
FeK	00.35	00.32
NiK	92.55	79.54

Figure S3. EDX analysis of 0.5%Ru/NiFe LDH-F/NF catalyst.

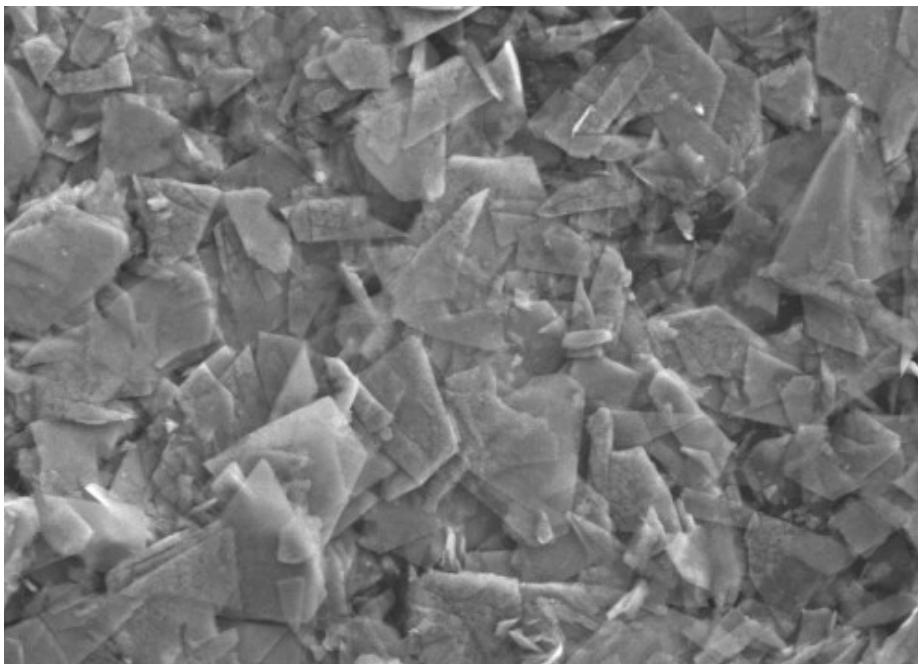

Figure S4. SEM image of Ru/NiFe LDH-F/NF catalyst.

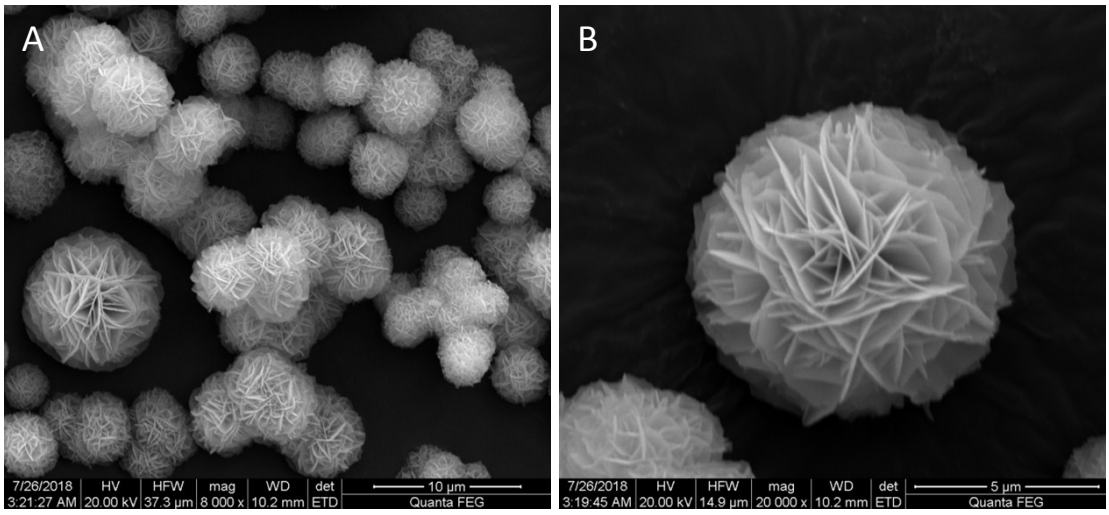

Figure S5. SEM image of NiFe LDH-F catalyst.

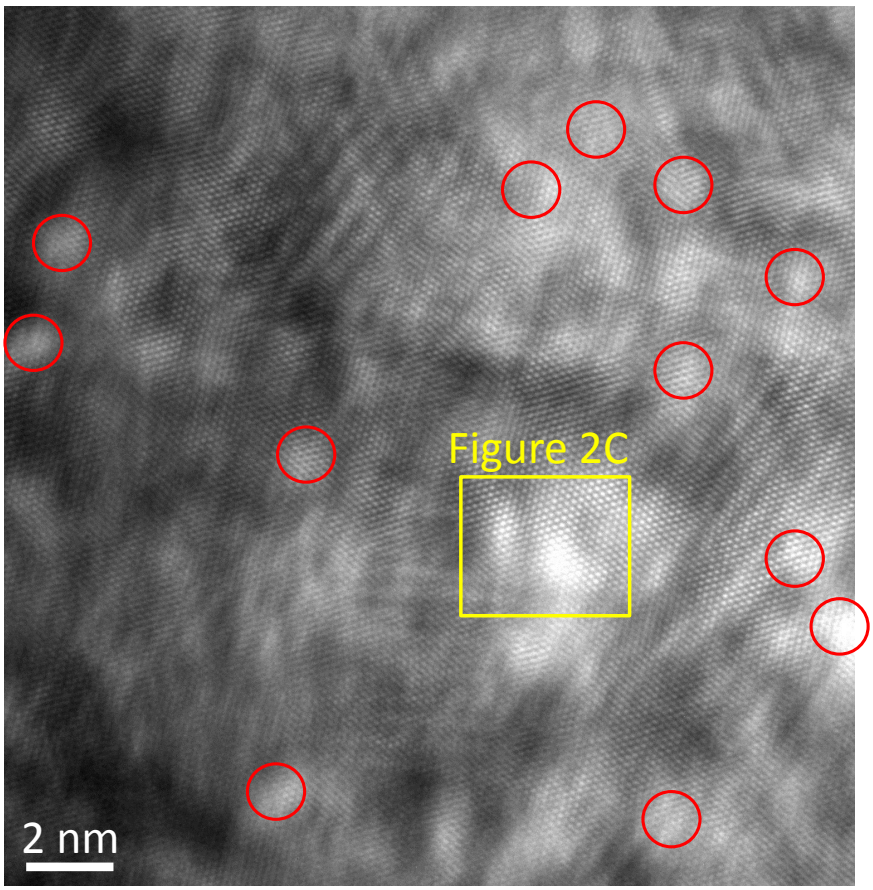

Figure S6. High-resolution TEM image of local domain of Ru/NiFe LDH-F nanosheets.

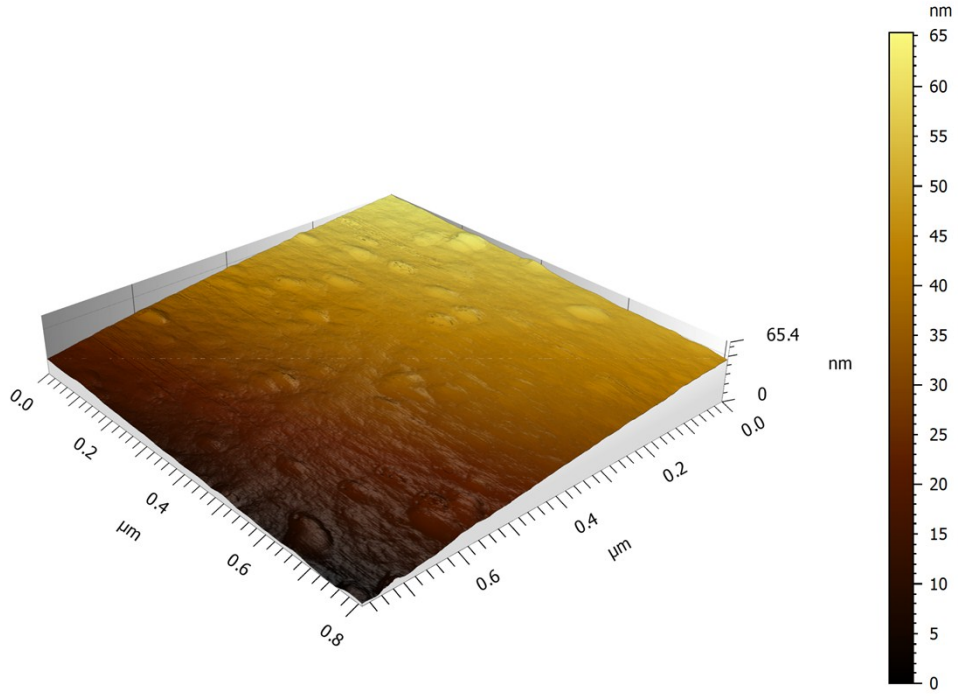

Figure S7. AFM image of Ru/NiFe LDH-F/NF catalyst.

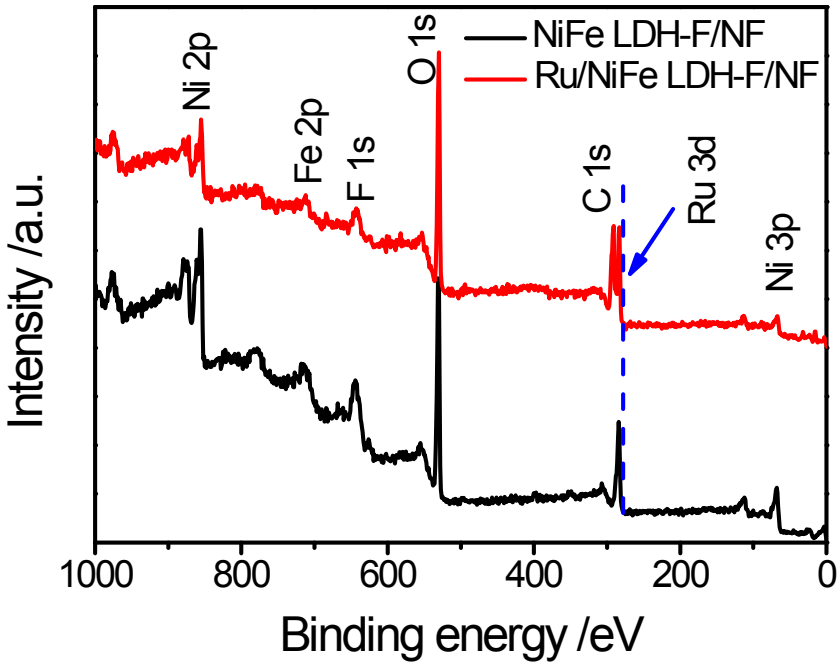

Figure S8. XPS patterns of the as-prepared Ru/NiFe LDH-F/NF and NiFe LDH-F/NF catalysts.

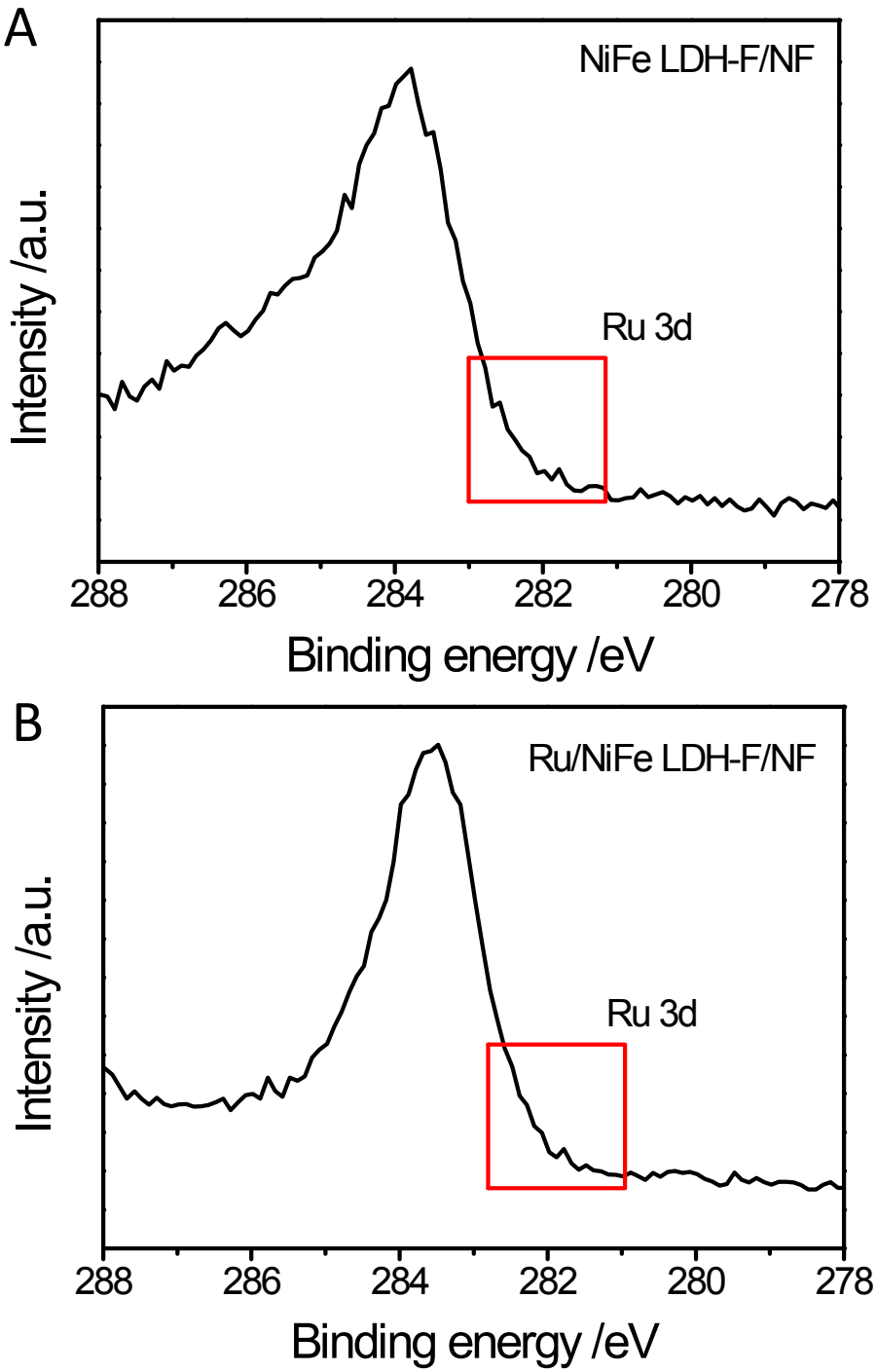

Figure S9. XPS patterns of the Ru 3d of the as-prepared (A) NiFe LDH-F/NF and (B) Ru/NiFe LDH-F/NF catalysts.

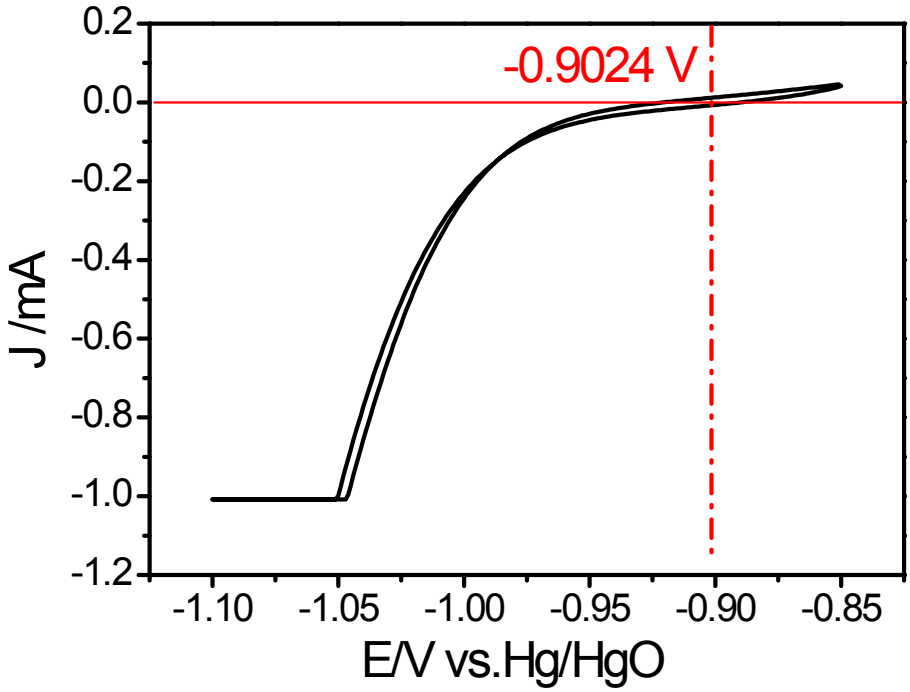

Figure S10. The CV curves (1 mV s^{-1}) of the calibration of the HgO/Hg reference electrode in 1 M KOH solution.

The calibration was performed in the high purity oxygen saturated electrolyte with a Pt foil as the working electrode. The average (-0.9024 V) of the two potentials where the current crossed zero was taken to be the thermodynamic potential. So, the formula of $E_{(Hg/HgO)}$ converting to $E_{(RHE)}$ is as following: $E_{(RHE)} = E_{(Hg|HgO)} + 0.9024$.

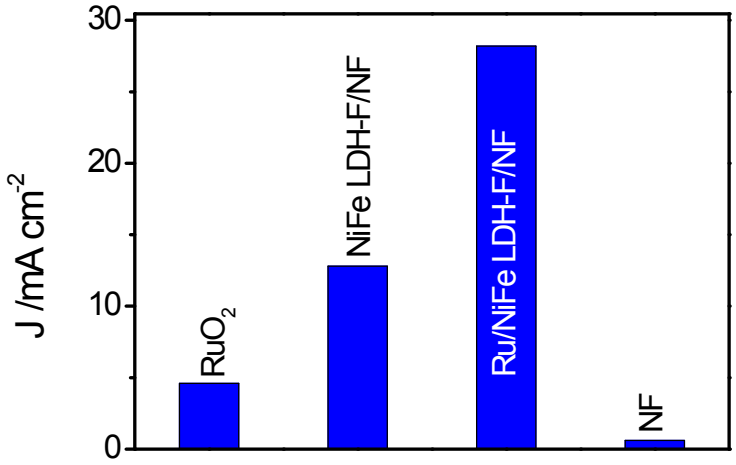

Figure S11. Comparison of OER current densities of the catalysts at a potential of 1.5 V.

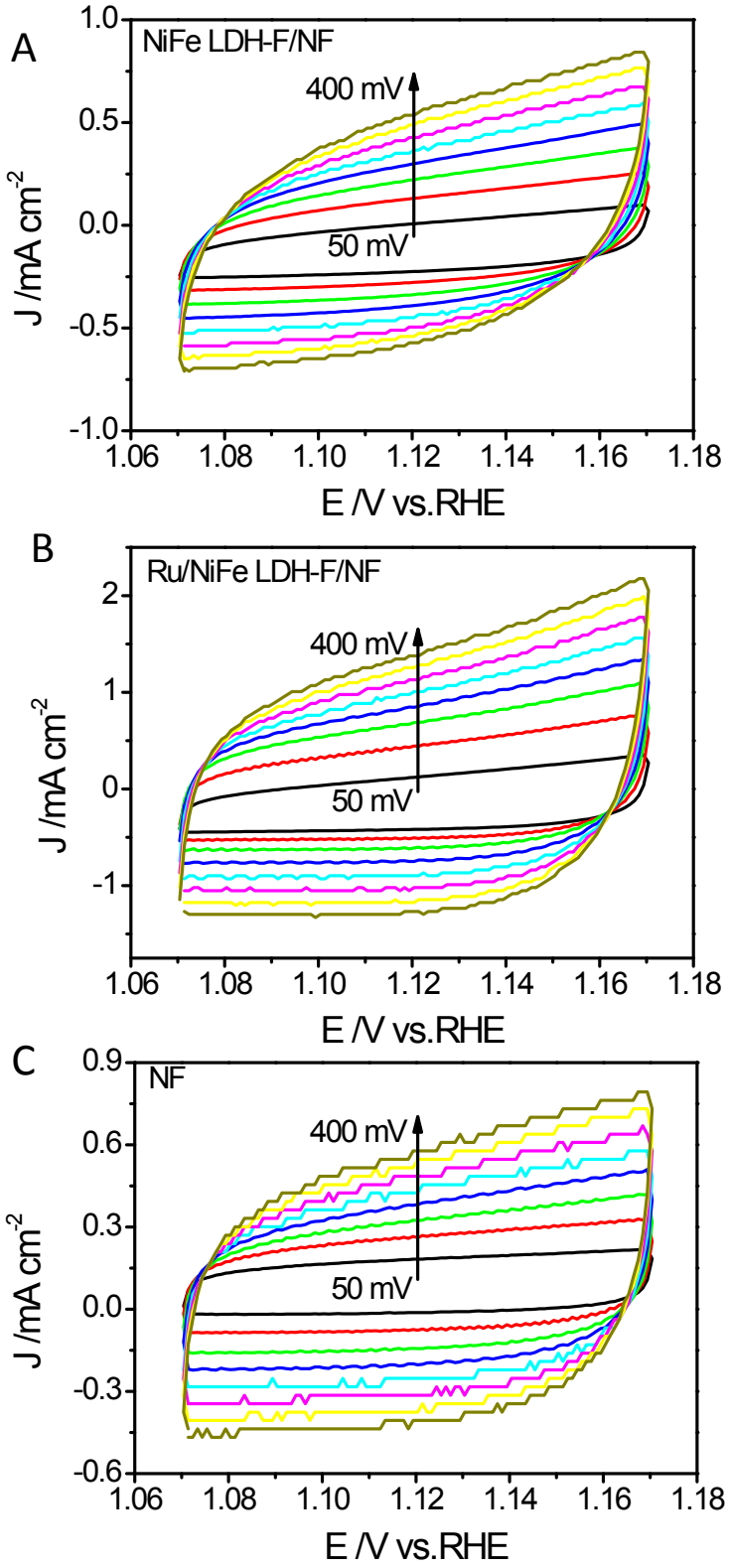

Figure S12. Electrochemical capacitance of (A) NiFe LDH-F/NF, (B) Ru/NiFe LDH-F/NF, and (C) NF measured in the non-Faradaic potential range at scan rates of 50, 100, 150, 200, 250, 300, 350, 400 mV s^{-1}, respectively.

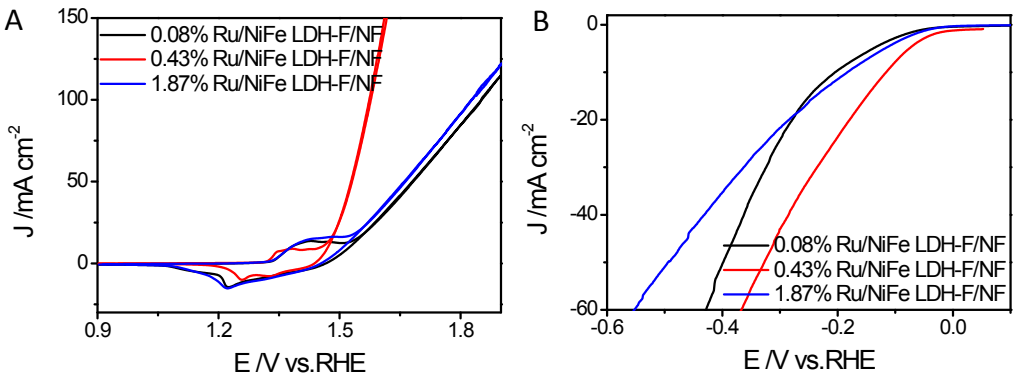

Figure S13. (A) OER LSV plots (B) OER LSV plots for different electrocatalysts.

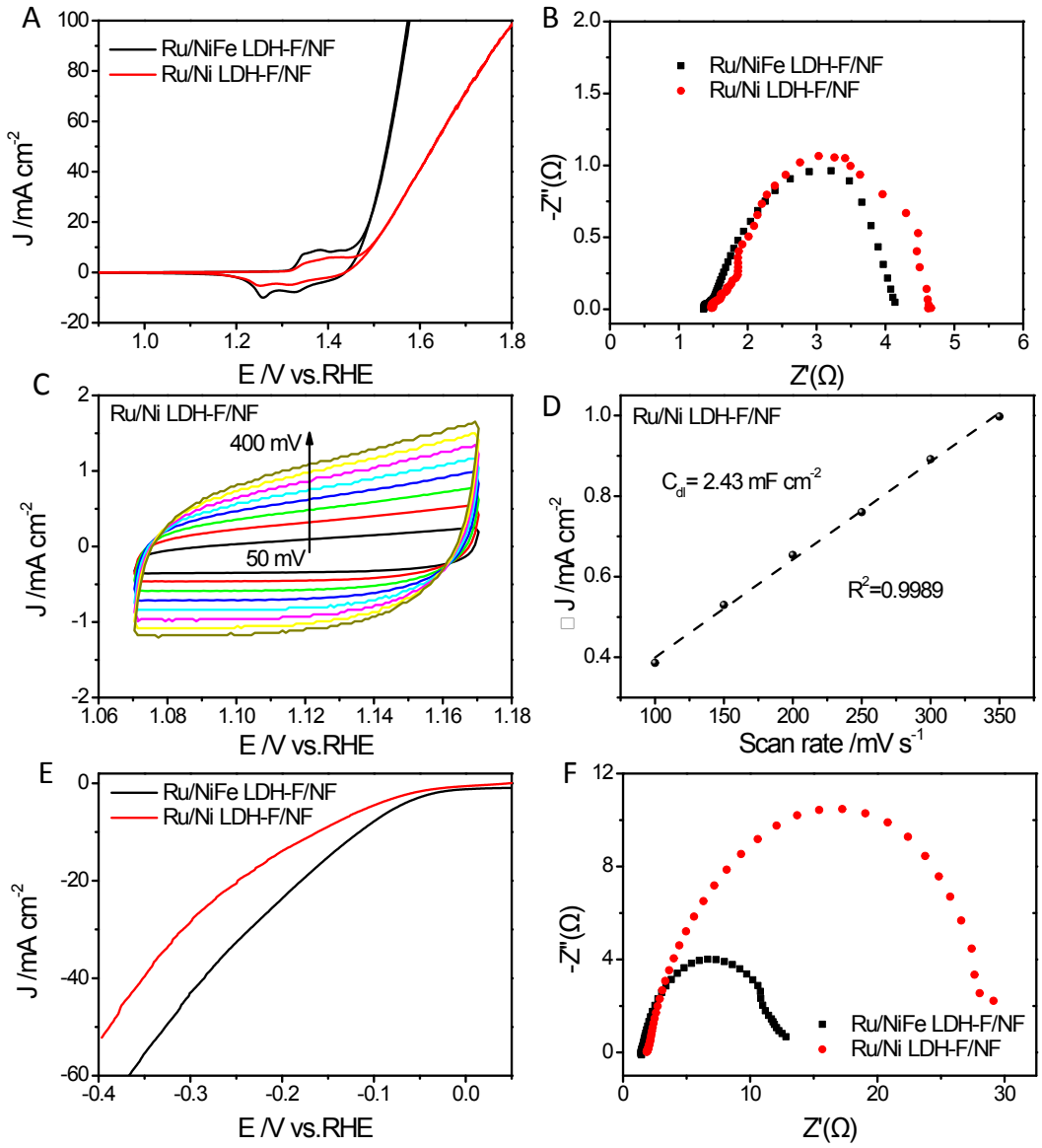

Figure S14. (A) OER LSV curves, (B) EIS curves recorded at 1.50 V vs. RHE of Ru/NiFe LDH-F/NF and Ru/Ni LDH-F/NF catalysts. (C) Electrochemical capacitance, (D) Linear fitting of the capacitive currents versus CV scan rates of Ru/Ni LDH-F/NF catalyst. (E) HER LSV curves, (F) EIS curves recorded at -0.1 V vs. RHE of Ru/NiFe LDH-F/NF and Ru/Ni LDH-F/NF catalysts.

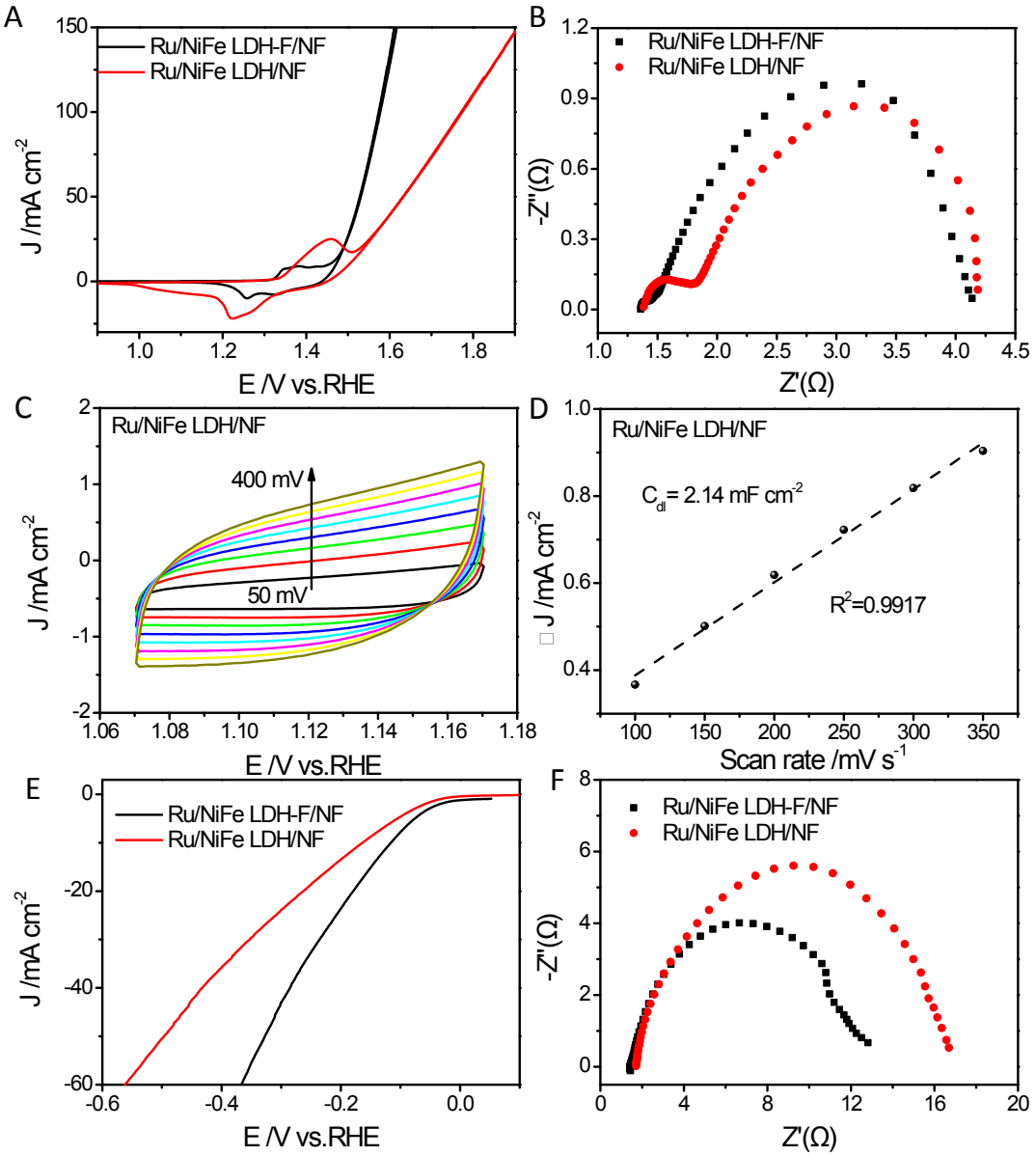

Figure S15. (A) OER LSV curves, (B) EIS curves recorded at 1.50 V vs. RHE of Ru/NiFe LDH-F/NF and Ru/NiFe LDH/NF catalysts. (C) Electrochemical capacitance, (D) Linear fitting of the capacitive currents versus CV scan rates of Ru/NiFe LDH/NF catalyst. (E) HER LSV curves, (F) EIS curves recorded at -0.1 V vs. RHE of Ru/NiFe LDH-F/NF and Ru/NiFe LDH/NF catalysts.

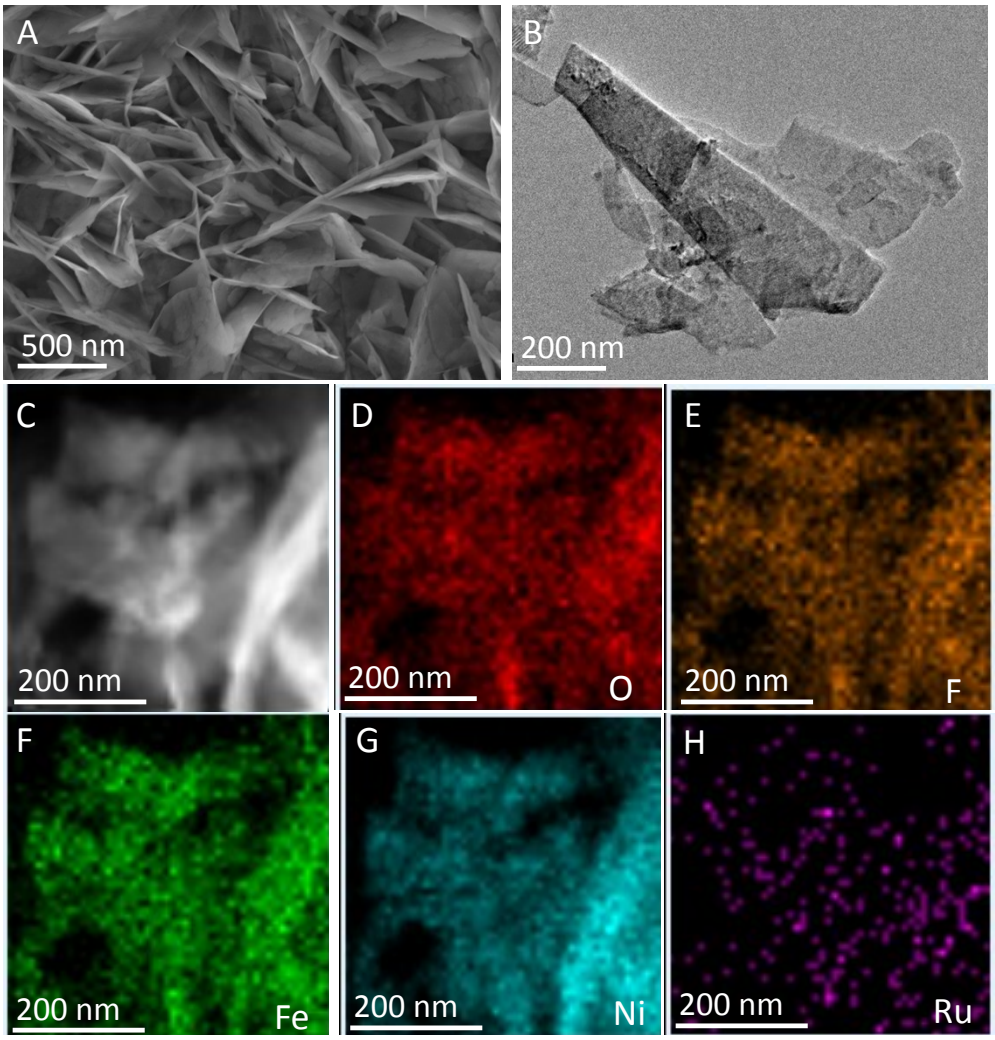

Figure S16. (A) SEM, (B) TEM and (C-H) EDS elemental mapping images of Ru/NiFe LDH/NF catalyst after stability test.

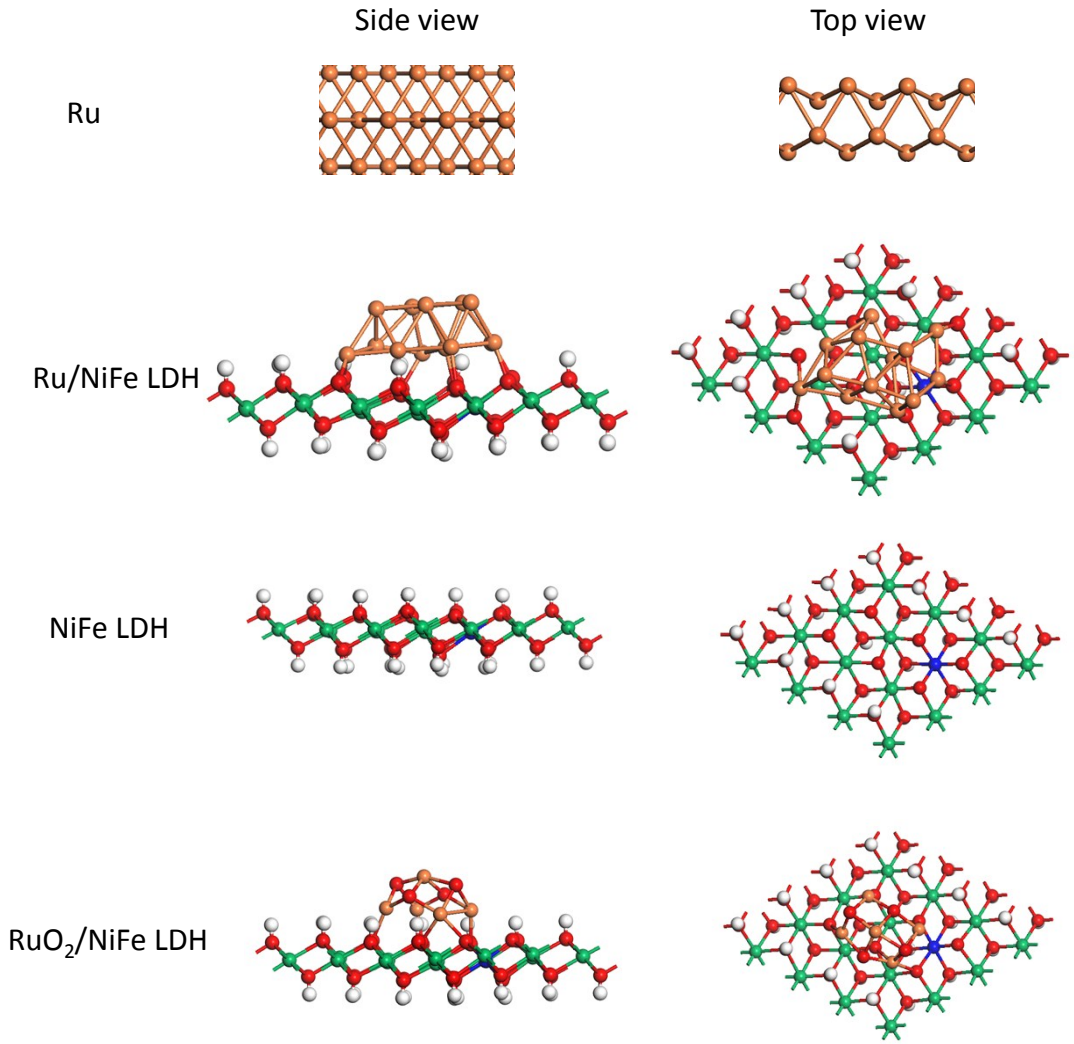

Figure S17. Structure models of Ru, Ru/NiFe LDH, NiFe LDH and RuO_2/NiFe LDH catalysts. Color code for atoms: Orange, Ru; blue, Fe; green, Ni; red: O; and white: H.

Table S1. Comparison of recent electrocatalysts for overall water splitting in alkaline electrolytes.

Electrocatalysts	Electrolyte	HER η_{10} (mV)	HER Tafel slop (mV dec^{-1})	OER η10 (mV)	OER Tafel slop (mV dec^{-1})	E_{10} (V)	**Ref.**
Ru/NiFe LDH-F/NF	1.0 M KOH	115.6	65.7	230	50.2	/	**This work**
RuO_2/NiO/NF	1.0 M KOH	22	31.7	250	50.5	1.5	**R1**
MoS_2-Ni_3S_2 HNRs/NF	1.0 M KOH	98	61	249	57	1.5	**R2**
NiO/Ni	1.0 M KOH	121	88	294	41	1.7	**R3**
$Co(SxSe1-x)_2$	1.0 M KOH	122	85.7	283	65.6	1.63	**R4**
FeB_2-NF	1.0 M KOH	61	87.5	296	52.4	1.57	**R5**
RuO_2/Co_3O_4	1.0 M KOH	89	91	305	69	1.645	**R6**
1D-RuO_2-CN_x	0.5 M KOH	95	70	260	56	/	**R7**
CoFePO/NF	1.0 M KOH	87.5	38.1	274.5	51.7	1.588	**R8**
NiCoFe LTHs/CFC	1.0 M KOH	200	70	239	32	1.55	**R9**
Ni_xP_y-325	1.0 M KOH	η_{20}=160	107.3	320	72.2	1.57	**R10**
Porous MoO_2/NF	1.0 M KOH	27	41	260	54	1.53	**R11**
$NiCo_2O_4$	1.0 M KOH	110	49.7	290	53	1.65	**R12**
2-cycle $NiFeO_x$/CFP	1.0 M KOH	88	150.2	250	31.5	1.55	**R13**
NiFe-LDH-NS@DG	1.0 M KOH	/	/	/	/	1.5	**R14**
Cu@NiFe LDH	1.0 M KOH	116	58.9	199	27.8	1.54	**R15**
Ni_5P_4 films	1.0 M KOH	/	/	/	/	1.70	**R16**
NiSe Nanowires/Ni foam	1.0 M KOH	/	/	/	/	1.63	**R17**
NiFe LDHs/NF	1.0 M KOH	/	/	/	/	1.70	**R18**
$Ni(OH)_2$/NF	1.0 M KOH	/	/	/	/	1.82	**R18**
NiMo HNRs	1.0 M KOH	/	/	/	/	1.64	**R19**
$RuO_2/TiM_{II}Pt/C/Ti$ M	1.0 M KOH	/	/	/	/	1.57	**R19**
Ni_2P	1.0 M KOH	/	/	/	/	1.63	**R20**
CoP films	1.0 M KOH	/	/	/	/	1.63	**R21**

Table S2. Comparison of the OER performance of the electrocatalysts in 1 M KOH.

Electrocatalysts	Overpotential (mV) (j =10 mAcm^{-2})	OER Tafel slop (mV dec^{-1})	**Ref.**
Ni-Fe MOF NSs	240	34	**R22**
$Na_{0.08}Ni_{0.9}Fe_{0.1}O_2$	260	44	**R23**
Li^+ converted $NiFeO_x$	230	31.5	**R13**
CoSe/NiFe LDH	250	57	**R24**
FeNi-LDH	224	52.8	**R25**
NiFe-LDH/CNT	247	31	**R26**
FeNi LDH	227	38	**R27**
NiFe LDH	280	50	**R28**

Table S3. Comparison of the HER performance of the electrocatalysts in 1 M KOH.

Electrocatalysts	Overpotential (mV) (j =10 mAcm^{-2})	Loading (mg cm^{-2})	**Ref.**
NiCoFe LTHs/CFC	200	0.4	**R9**
Ni nanowires	350	1.0	**R29**
Bulk MoB	225	0.5	**R30**
Bulk Mo_2C	195	0.8	**R30**
Porous $NiSe_2$ nanosheets	184	0.46	**R31**
Ni_5P_4 Films	150	/	**R32**
CoP/CC	209	0.92	**R33**
Ni_2P	220	5.0	**R20**
NiFe LDHs	219	N.A.	**R34**
MoC_x	151	0.8	**R35**
Co NPs@N-CNTs	370	0.28	**R36**
NiFe-LDH-NS@DG	300	0.28	**R14**
Cu@NiFe LDH	116	2.2	**R15**
NiO/Ni-CNT	< 100	0.28	**R39**

Table S4. Actual metal loading of each catalyst, determined by ICP-OES.

Catalysts	Ni (actual loading)	Fe (actual loading)	Ru (actual loading)
NiFe LDH-F/NF	89.24%	10.76%	/
0.08%Ru/NiFe LDH-F/NF	88.70%	11.22%	0.08%
0.43%Ru/NiFe LDH-F/NF	89.01%	10.56%	0.43%
1.87%Ru/NiFe LDH-F/NF	88.21%	9.92%	1.87%

Note: The net weight of NiFe LDH-F/NF, 0.1%Ru/NiFe LDH-F/NF, 0.5%Ru/NiFe LDH-F/NF, and 2%Ru/NiFe LDH-F/NF are about 2 mg. In order to ICP test, the nanosheets of as-prepared catalysts were scratched off the NF and collected by sonication method 30 min.

Reference

R1. Liu, J.; Zheng, Y.; Jiao, Y.; Wang, Z.; Lu, Z.; Vasileff, A.; Qiao, S.-Z., NiO as a Bifunctional promoter for RuO_2 toward superior overall water splitting. *Small* **2018,** *14*, 1704073.

R2. Yang, Y.; Zhang, K.; Ling, H.; Li, X.; Chan, H. C.; Yang, L.; Gao, Q., MoS_2-Ni_3S_2 heteronanorods as efficient and stable bifunctional electrocatalysts for overall water splitting. *ACS Catal.* **2017,** *7*, 2357-2366.

R3. Ou, G.; Fan, P.; Zhang, H.; Huang, K.; Yang, C.; Yu, W.; Wei, H.; Zhong, M.; Wu, H.; Li, Y., Large-scale hierarchical oxide nanostructures for high-performance electrocatalytic water splitting. *Nano Energy* **2017,** *35*, 207-214.

R4. Fang, L.; Li, W.; Guan, Y.; Feng, Y.; Zhang, H.; Wang, S.; Wang, Y., Tuning unique peapod-like $Co(S_xSe_{1-x})_2$ nanoparticles for efficient overall water splitting. *Adv. Funct. Mater.* **2017,** *27*, 2071008.

R5. Li, H.; Wen, P.; Li, Q.; Dun, C.; Xing, J.; Lu, C.; Adhikari, S.; Jiang, L.; Carroll, D. L.; Geyer, S. M. Earth-abundant iron diboride (FeB_2) nanoparticles as highly active bifunctional electrocatalysts for overall water splitting. *Adv. Energy Mater.* **2017**, *7*, 1700513.

R6. Liu, H.; Xia, G.; Zhang, R.; Jiang, P.; Chen, J.; Chen, Q., MOF-derived RuO_2/Co_3O_4 heterojunctions as highly efficient bifunctional electrocatalysts for HER and OER in alkaline solutions. *RSC Adv.* **2017,** *7*, 3686-3694.

R7. Bhowmik, T.; Kundu, M. K.; Barman, S., Growth of one-dimensional RuO_2 nanowires on g-carbon nitride: an active and stable bifunctional electrocatalyst for hydrogen and oxygen evolution reactions at all pH values. *ACS Appl. Mater. Inter.* **2016,** *8*, 28678-28688.

R8. Duan, J.; Chen, S.; Vasileff, A.; Qiao, S. Z., Anion and cation modulation in metal compounds for bifunctional overall water splitting. *ACS Nano* **2016,** *10*, 8738-8745.

R9. Wang, A.-L.; Xu, H.; Li, G.-R., NiCoFe layered triple hydroxides with porous structures as high-performance electrocatalysts for overall water splitting. *ACS Energ. Lett.* **2016,** *1*, 445-453.

R10. Li, J.; Li, J.; Zhou, X.; Xia, Z.; Gao, W.; Ma, Y.; Qu, Y., Highly efficient and robust nickel phosphides as bifunctional electrocatalysts for overall water-splitting. *ACS Appl. Mater. Inter.* **2016,** *8*, 10826-10834.

R11. Jin, Y.; Wang, H.; Li, J.; Yue, X.; Han, Y.; Shen, P. K.; Cui, Y., Porous MoO_2 nanosheets as non-noble bifunctional electrocatalysts for overall water splitting. *Adv. Mater.* **2016,** *28*, 3785-3790.

R12. Gao, X.; Zhang, H.; Li, Q.; Yu, X.; Hong, Z.; Zhang, X.; Liang, C.; Lin, Z., Hierarchical $NiCo_2O_4$ hollow microcuboids as bifunctional electrocatalysts for overall water-splitting. *Angew. Chem. Int. Edit.* **2016,** *55*, 6290-6294.

R13. Wang, H.; Lee, H.-W.; Deng, Y.; Lu, Z.; Hsu, P.-C.; Liu, Y.; Lin, D.; Cui, Y., Bifunctional non-noble metal oxide nanoparticle electrocatalysts through lithium-induced conversion for overall water splitting. *Nat. Commun.* **2015,** *6*, 7261.

R14. Jia, Y.; Zhang, L.; Gao, G.; Chen, H.; Wang, B.; Zhou, J.; Soo, M. T.; Hong, M.; Yan, X.; Qian, G.; Zou, J.; Du, A.; Yao, X., A Heterostructure coupling of exfoliated Ni-Fe hydroxide nanosheet and defective graphene as a bifunctional electrocatalyst for overall water splitting. *Adv. Mater.* **2017,** *29*, 1700017.

R15. Yu, L.; Zhou, H.; Sun, J.; Qin, F.; Yu, F.; Bao, J.; Yu, Y.; Chen, S.; Ren, Z., Cu nanowires shelled with NiFe layered double hydroxide nanosheets as bifunctional electrocatalysts for overall water splitting. *Energ. Environ. Sci.* **2017,** *10*, 1820-1827.

R16. Ledendecker, M.; Calderon, S. K.; Papp, C.; Steinrueck, H.-P.; Antonietti, M.; Shalom, M., The synthesis of nanostructured ni5p4 films and their use as a non-noble bifunctional electrocatalyst for full water splitting. *Angew. Chem. Int. Edit.* **2015,** *54*, 12361-12365.

R17. Tang, C.; Cheng, N.; Pu, Z.; Xing, W.; Sun, X., NiSe nanowire film supported on nickel foam: an efficient and stable 3d bifunctional electrode for full water splitting. *Angew. Chem. Int. Edit.* **2015,** *54*, 9351-9355.

R18. Luo, J.; Im, J.-H.; Mayer, M. T.; Schreier, M.; Nazeeruddin, M. K.; Park, N.-G.; Tilley, S. D.; Fan, H. J.; Graetzel, M., Water photolysis at 12.3% efficiency via perovskite photovoltaics and earth-abundant catalysts. *Science* **2014,** *345*, 1593-1596.

R19. Tian, J.; Cheng, N.; Liu, Q.; Sun, X.; He, Y.; Asiri, A. M., Self-supported NiMo hollow nanorod array: an efficient 3D bifunctional catalytic electrode for overall water splitting. *J. Mater. Chem. A* **2015,** *3*, 20056-20059.

R20. Stern, L.-A.; Feng, L.; Song, F.; Hu, X., Ni_2P as a Janus catalyst for water splitting: the oxygen evolution activity of Ni_2P nanoparticles. *Energ. Environ. Sci.* **2015,** *8*, 2347-2351.

R21. Jiang, N.; You, B.; Sheng, M.; Sun, Y., Electrodeposited cobalt-phosphorous-derived films as competent bifunctional catalysts for overall water splitting. *Angew. Chem. Int. Edit.* **2015,** *54*, 6251-6254.

R22. Zhang, N.; Cheng, F.; Liu, J.; Wang, L.; Long, X.; Liu, X.; Li, F.; Chen, J., Rechargeable aqueous zinc-manganese dioxide batteries with high energy and power densities. *Nat. Commun.* **2017,** *8*, 1-7.

R23. Yu, L.; Zhou, H.; Sun, J.; Qin, F.; Yu, F.; Bao, J.; Yu, Y.; Chen, S.; Ren, Z., Cu nanowires shelled with NiFe layered double hydroxide nanosheets as bifunctional electrocatalysts for overall water splitting. *Energ. Environ. Sci.* **2017,** *10*, 1820-1827.

R24. Hou, Y.; Lohe, M. R.; Zhang, j.; Liu, S.; Zhuang X.; and Feng, X. Vertically oriented cobalt selenide/NiFe layered-double-hydroxide nanosheets supported on exfoliated graphene foil: an efficient 3D electrode for overall water splitting. *Energ. Environ. Sci.*, **2016**, *9*, 478-483.

R25. Li, Z.; Shao, M.; An, H.; Wang, Z.; Xu, S.; Wei, M.; Evans, D. G.; Duan, X., Fast electrosynthesis of Fe-containing layered double hydroxide arrays toward highly efficient electrocatalytic oxidation reactions. *Chem. Sci.* **2015,** *6*, 6624-6631.

R26. Gong, M.; Li, Y.; Wang, H.; Liang, Y.; Wu, J. Z.; Zhou, J.; Wang, J.; Regier, T.;

Wei, F.; Dai, H., An advanced Ni-Fe layered double hydroxide electrocatalyst for water oxidation. *J. Am. Chem. Soc.* **2013,** *135*, 8452-8455.

R27. Long, X.; Ma, Z.; Yu, H.; Gao, X.; Pan, X.; Chen, X.; Yang, S.; Yi, Z., Porous FeNi oxide nanosheets as advanced electrochemical catalysts for sustained water oxidation. *J. Mater. Chem. A* **2016,** *4*, 14939-14943.

R28. Lu, Z.; Xu, W.; Zhu, W.; Yang, Q.; Lei, X.; Liu, J.; Li, Y.; Sun, X.; Duan, X., Three-dimensional NiFe layered double hydroxide film for high-efficiency oxygen evolution reaction. *Chem. Commun.* **2014,** *50*, 6479-6482.

R29. McKone, J. R.; Sadtler, B. F.; Werlang, C. A.; Lewis, N. S.; Gray, H. B., Ni-Mo Nanopowders for Efficient Electrochemical Hydrogen Evolution. *ACS Catal.* **2013,** *3*, 166-169.

R30. Vrubel, H.; Hu, X., Molybdenum boride and carbide catalyze hydrogen evolution in both acidic and basic solutions. *Angew. Chem. Int. Edit.* **2012,** *51*, 12703-12706.

R31. Liang, H.; Li, L.; Meng, F.; Dang, L.; Zhuo, J.; Forticaux, A.; Wang, Z.; Jin, S., Porous two-dimensional nanosheets converted from layered double hydroxides and their applications in electrocatalytic water splitting. *Chem. Mater.* **2015,** *27*, 5702-5711.

R32. Ledendecker, M.; Calderon, S. K.; Papp, C.; Steinrueck, H.-P.; Antonietti, M.; Shalom, M., The synthesis of nanostructured ni_5p_4 films and their use as a non-noble bifunctional electrocatalyst for full water splitting. *Angew. Chem. Int. Edit.* **2015,** *54*, 12361-12365.

R33. Tian, J.; Liu, Q.; Asiri, A. M.; Sun, X., Self-supported nanoporous cobalt phosphide nanowire arrays: an efficient 3d hydrogen-evolving cathode over the wide range of pH 0-14. *J. Am. Chem. Soc.* **2014,** *136*, 7587-7590.

R34. Luo, J.; Im, J.-H.; Mayer, M. T.; Schreier, M.; Nazeeruddin, M. K.; Park, N.-G.; Tilley, S. D.; Fan, H. J.; Graetzel, M., Water photolysis at 12.3% efficiency via perovskite photovoltaics and Earth-abundant catalysts. *Science* **2014,** *345*, 1593-1596.

R35. Wang, H.; Lee, H.-W.; Deng, Y.; Lu, Z.; Hsu, P.-C.; Liu, Y.; Lin, D.; Cui, Y., Bifunctional non-noble metal oxide nanoparticle electrocatalysts through lithium-induced conversion for overall water splitting. *Nat. Commun.* **2015,** *6*, 6512.

R36. Zou, X.; Huang, X.; Goswami, A.; Silva, R.; Sathe, B. R.; Mikmekova, E.; Asefa, T., Cobalt-embedded nitrogen-rich carbon nanotubes efficiently catalyze hydrogen evolution reaction at all pH values. *Angew. Chem. Int. Edit.* **2014,** *53*, 4372-4376.

R37. Gong, M.; Zhou, W.; Tsai, M.-C.; Zhou, J.; Guan, M.; Lin, M.-C.; Zhang, B.; Hu, Y.; Wang, D.-Y.; Yang, J.; Pennycook, S. J.; Hwang, B.-J.; Dai, H., Nanoscale nickel oxide/nickel heterostructures for active hydrogen evolution electrocatalysis. *Nat. Commun.* **2014,** *5*, 4695.